Optical Heterodyne Millimeter-Wave Generation Using 1.55-μm Traveling-Wave Photodetectors

Andreas Stöhr, *Member, IEEE,* Robert Heinzelmann, Andrei Malcoci, and Dieter Jäger, *Fellow, IEEE*

***Abstract*—Optical heterodyne millimeter-wave generation using traveling-wave photodetectors (TW-PDs) is examined both experimentally and theoretically. Ultrahigh-frequency InP-based 1.55-μm TW-PDs were fabricated and employed in an experimental setup for optical heterodyning. For the first time, optical heterodyne millimeter-wave generation in excess of 160 GHz is experimentally demonstrated in frequency domain. The maximum electrical power delivered by the TW-PD to a 5052 impedance is −11.5 dBm at 110 GHz with a polarization penalty of only 1.3 dB. Furthermore, a theoretical analysis in frequency domain is presented describing the frequency response of TW-PD including effects of the photogenerated carrier dynamics as well as optical and electrical wave propagation phenomena. A broad-band and flat frequency response is found indicating a total rolloff of about 13.1 dB for a frequency span from 25 GHz to 200 GHz. Finally, the detectors responsivity is theoretically investigated to differentiate between the physical phenomena associated with high-frequency limitations.**

***Index Terms*—Light polarization, microwave photonics, millimeter wave generation, optical heterodyne, photodetector, p-i-n photodiodes, semiconductor device modeling.**

I. Introduction

OPTICAL HETERODYNE generation of high-power millimeter- and submillimeter-wave signals using ultrahigh-frequency photodetectors is a promising technique for radio astronomy and wireless broad-band communications. From first ideas and concepts, published about 20 years ago [1], an enormous progress has been made up to now. Especially, in the last few years this progress has significantly been pushed from the application side, i.e., from interest in developing systems such as large (sub)millimeter-wave antenna arrays [2] or millimeter-wave fiber-radio systems [3], [4]. In such systems, high-frequency (sub)millimeter-wave local oscillator (LO) signals must be distributed to remote antenna stations. Since this is not feasible by electrical means due to the high propagation loss of electrical waveguides at (sub)millimeter-wave frequencies, so-called "photonic LOs" are required. The preferred operation wavelength of such a photonic LO was found to be within the 1.55-μm window due to the minimum transmission loss of the optical fiber and the availability of high-power erbium-doped fiber amplifiers, tunable laser diodes and other required fiber components [2].

Manuscript received January 22, 2001; revised May 24, 2001. This work was supported by the European Southern Observatory (ESO) under Contract 59608/MAP/00/6750/RFI within the ALMA Project.

The authors are with Gerhard-Mercator-Universität Duisburg, ZHO-Optoelektronik, 47057 Duisburg, Germany.

Publisher Item Identifier S 0018-9480(01)08704-X.

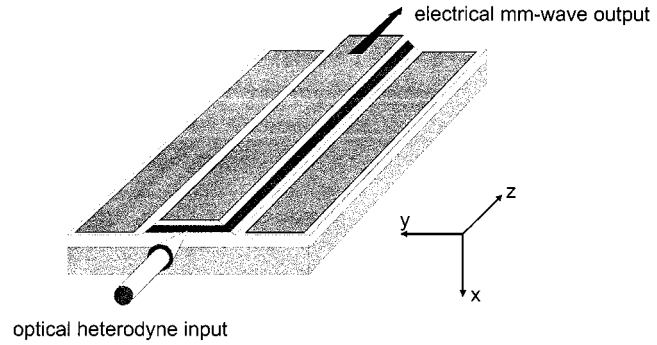

Fig. 1. Schematic diagram of the fabricated 1.55-μm TW-PD.

To date, there have been just a few experimental reports on ultrahigh-frequency 1.55-μm photodetectors for optical heterodyne millimeter-wave generation. In general, the fabricated devices can be separated into lumped [5], [6] and distributed detectors [7]–[9]. Among the lumped elements the uni-traveling-carrier (UTC) detectors are the most promising approach and UTC detectors have been reported for continuous wave (CW) optical heterodyne frequency generation up to 120 GHz [6]. In [8], a cascaded velocity matched 1.55-μm detector for W-band operation up to 105 GHz is reported and we demonstrated broad-band optical heterodyne millimeter-wave generation up 110 GHz using a 1.55-μm traveling-wave photodetector (TW-PD) [9]. This paper reports on the fabrication and experimental verification of an ultrahigh-frequency ($>$160 GHz) 1.55 -μm TW-PD for high-power millimeter-wave generation. Optical saturation effects as well as the polarization dependence of the detector are experimentally investigated. Furthermore, a theoretical analysis is presented describing the frequency response of the fabricated TW-PD including dynamic effects of the photogenerated carrier as well as wave propagation phenomena.

II. TW-PD

A sketch of the 50-μm-long TW-PD for optical heterodyne millimeter-wave generation investigated in this paper is shown in Fig. 1. The detector consists of an optical channel waveguide and an electrical transmission line. The optical heterodyne signal launched into the optical channel waveguide is gradually absorbed resulting in a distributed current generation along the detectors length that contributes to the overall current propagating along the electrical transmission line of the TW-PD. The traveling-wave detector differs from a lumped element in

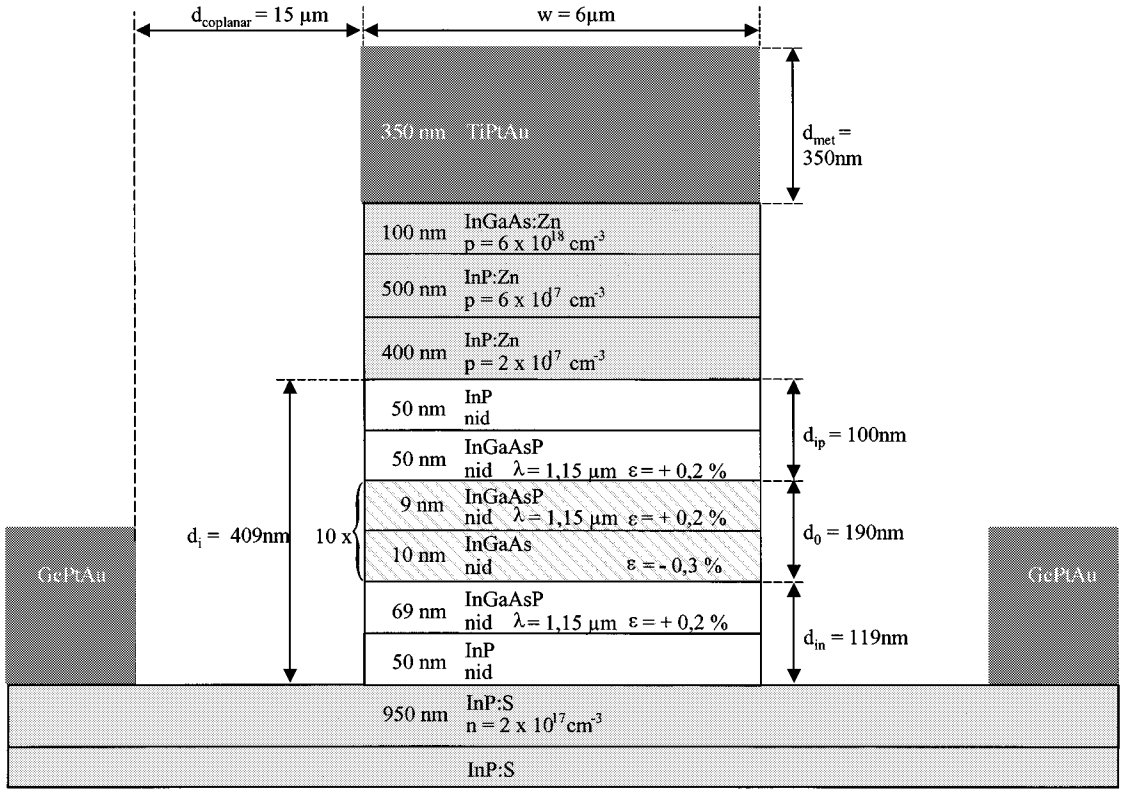

Fig. 2. Detailed cross section of the fabricated TW-PD.

a non-*RC* time limited response exhibiting superior high-frequency performances which has been recently demonstrated experimentally [7]–[9].

A cross section including the relevant geometrical parameters of the TW-PD investigated in this paper is shown in Fig. 2. The waveguide structure was grown on InP : S substrate by metalorganic vapor phase epitaxy. The optical core is embedded in the intrinsic region of a p-i-n diode. The absorptive region of the optical core consists of a multiple-quantum-well (MQW) section. A small strain is applied to the wells and the barriers of the MQW section to reduce the splitting of the valence band degeneracy resulting in identical electroabsorption properties for both the TM and TE modes. This way, the waveguide core of the TW-PD exhibits a polarization insensitive absorption coefficient at 1.55-μm wavelength. In detail, the waveguide core mainly consists of ten periods of 10-nm 0.3% tensile strained InGaAs QWs separated by 9-nm-thick 0.2% compressively strained 1.15-μm InGaAsP barriers. To increase fiber-to-chip coupling efficiency the overall thickness of the optical core is increased by transparent 1.15-μm quaternary InGaAsP layers adjacent to the MQW-region. The waveguide cladding layers consist of p- and n-doped InP together with 50 nm of nonintentionally doped InP layers adjacent to the core. The undoped InP sections prevent diffusion of the dopants into the waveguide core and therefore increase the total thickness of the intrinsic region to $d_i = 409$ nm. On top of the upper cladding a thin p-doped lattice matched InGaAs contact layer finalizes the optical waveguide structure.

The technological realization of the optical waveguide together with the hybrid microstrip/coplanar transmission line consists of a self aligned etching process and two metallization steps for the p- and n-type ohmic contacts. At first e-beam evaporation of the p-type TiPtAu center contact is performed which is also used as a mask for the subsequent etching processes of the waveguide mesa. Selective wet-chemical etching of the contact layer, the top cladding and the optical waveguide region is performed followed by the GePtAu metallization to form the n-type ground contact of the electrical waveguide.

III. Optical Heterodyne Measurements

The frequency response of the fabricated TW-PD is characterized using an experimental setup for optical heterodyning with two 1.55-μm CW laser diodes. The beat frequency f_{RF} of the generated RF signal can be tuned by varying the wavelength of the first laser λ_{tuned} while keeping the wavelength λ_0 of the second laser fixed

$$f_{\mathrm{RF}} = c \cdot \left(\frac{1}{\lambda_0} - \frac{1}{\lambda_{\mathrm{tuned}}} \right). \tag{1}$$

A schematic of the experimental setup can be found in [9]. The linear polarized optical output signals of two free-running external cavity laser diodes are combined using a 3-dB optical coupler. The polarization state of both lasers is adjusted to each other by tuning the polarization state of the tuned laser using a polarization controller. The combined optical heterodyne signal is amplified by a high-power erbium-doped fiber amplifier (EDFA). A variable optical attenuator is employed for performing power dependent measurements. A second polarization controller is used to adjust the input polarization heterodyne

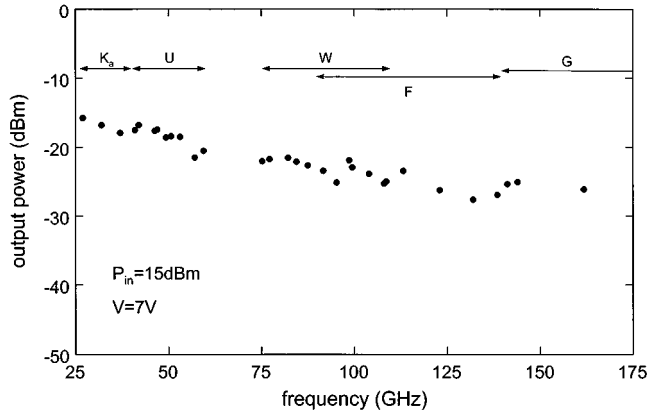

Fig. 3. Broad-band K_a- to G-band millimeter-wave generation using the TW-PD. The associated frequency bands of the applied coplanar probes and mixers are shown.

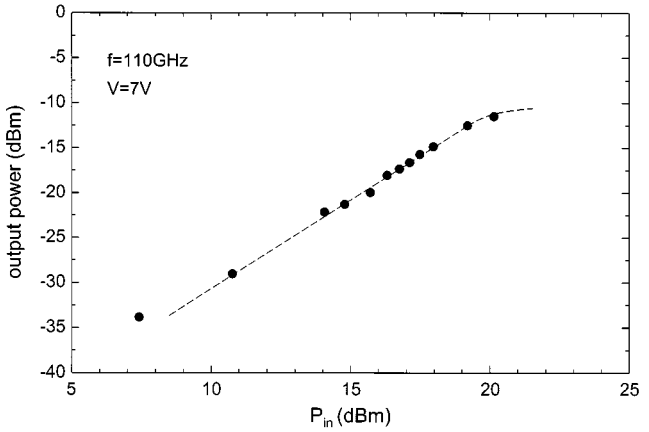

Fig. 4. Generated millimeter-wave power at 110 GHz versus the optical input power.

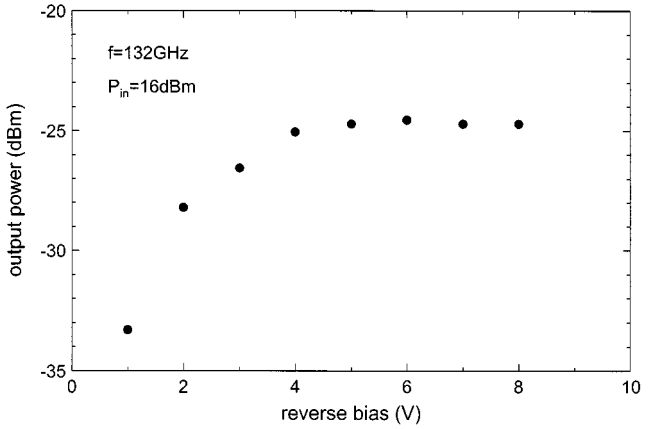

Fig. 5. Generated millimeter-wave power at 132 GHz versus the applied reverse bias.

optical signal to determine the polarization dependence of the RF output signal. Optical input power to the TW-PD is monitored by coupling 5% of the optical heterodyne signal to a dual-purpose optical spectrum analyzer/power meter. The TW-PD is reverse biased using a dc voltage source with internal current monitoring. A cleaved optical single mode fiber is used for fiber-to-chip coupling. For on-wafer measurements over the wide frequency span up to 160 GHz different calibrated coplanar probes are used. For frequencies up to 50 GHz the generated electrical power is directly measured using a millimeter-wave spectrum analyzer. Measurements at frequencies within the U-, W-, F-, and G-bands are performed utilizing the calibrated external mixers.

The active waveguide section of the TW-PD investigated in this work was 50-μm long with a width of 6 μm. The device exhibits a dc responsivity of 0.2 A/W at a reverse bias of 7 V and a maximum breakdown voltage in excess of 9 V. Frequency response measurements were performed keeping a fixed optical wavelength of 1.54 μm, while tuning the other laser toward larger wavelengths. A reverse bias of 7 V was applied to the TW-PD and the overall optical input power was set to $+15$ dBm ($+12$ dBm per carrier).

The measured frequency response from 25 GHz to 160 GHz is shown in Fig. 3. As can be seen, a flat and broad-band frequency response is achieved with a total signal rolloff from 25 to 160 GHz of about 10 dB. To our knowledge, this is the first time optical heterodyne CW millimeter-wave generation using a photodetector is demonstrated up to 160 GHz. The different physical phenomena contributing to the overall rolloff of the TW-PD are discussed in detail in Section IV.

In Fig. 4, the measured millimeter-wave output power at a beat frequency of 110 GHz is plotted versus the optical input power. A maximum millimeter-wave power level of -11.5 dBm is achieved representing the highest millimeter-wave power level ever reported for 1.55-μm waveguide photodetectors. Furthermore, it should be noted that the power delivered to the 50 Ω probe is measured. The total power generated by the TW-PD is about 8 dB larger as will be explained in the next section. No saturation effects are observed up to electrical power levels of -13 dBm where electrical millimeter-wave power exhibits the expected quadratic dependence on the optical input power. At electrical power levels in excess of -13-dBm saturation effects can be observed.

The power conversion efficiency of the investigated TW-PD is bias dependent as can be seen from Fig. 5. Here, the measured millimeter-wave power at a beat frequency of 132 GHz is shown versus the applied reverse bias. Clearly, the generated power gets smaller if the reverse bias is reduced below 4 V. Previous experiments have already shown that the nonlinear saturation behavior of ultrahigh frequency p-i-n photodetectors under high power illumination can be overcome by applying a large external bias [8]–[10]. Physically, the nonlinear power dependence is mainly attributed to a reduced carrier velocity in the intrinsic waveguide core of the detector. The photogenerated carriers induce a space charge field reducing or even screening out the applied bias field at low biases and thus resulting in a significantly reduced carrier velocity [10]. According to equations given in [1], the generated space charge field in the investigated TW-PD can be estimated to be in the order of 20–30 kV/cm. Thus, for reverse voltages below 4 V the space charge field screens out the applied bias field leading to saturation effects due to reduced electron and hole velocities.

Finally, the dependence of the conversion efficiency was investigated. For this purpose the polarization angle of the linear polarized input signal was rotated using a halfwave plate

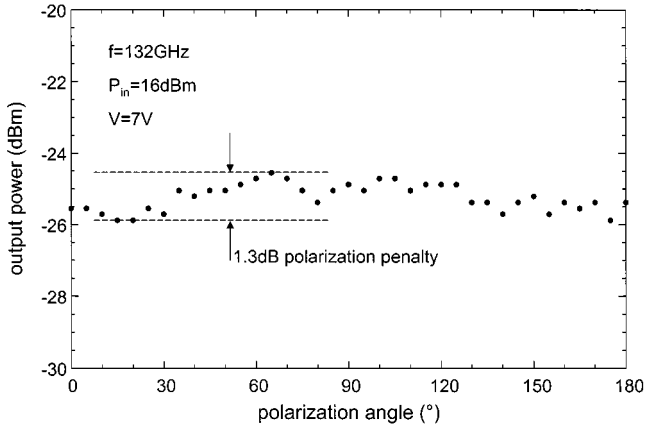

Fig. 6. Generated millimeter-wave power at 132 GHz versus the polarization angle.

inside the second polarization controller. In Fig. 6 the measured millimeter-wave power at a beat frequency of 132 GHz is shown versus the relative polarization angle of the heterodyne signal. As can be seen, the maximum polarization penalty is only 1.3 dB, which can be attributed to the polarization insensitive design of the absorption region by using strained QWs as discussed in Section II.

IV. Theoretical Analysis

In order to further improve the design of the TW-PD with respect to higher frequencies it is inevitable to identify the relevant physical effects limiting the frequency response of the TW-PD and to study the impact of design variations on the detector performance. For this purpose a theoretical analysis is developed in the following including all relevant phenomena of the photogenerated carriers together with optical and electrical wave propagation effects. Recently, several groups reported on theoretical studies on the high-frequency and high-current limitations of TW-PD. A time domain model describing the picosecond pulse response of a TW-PD has been reported in [11]. A first analytical description of a TW-PD in frequency domain can be found in [1]. This model describes the photogenerated current source per unit length and also includes wave propagation effects. However, this work did not consider velocity mismatch effects. Furthermore, the limitation due to the transit time was reduced to a single time constant similar to [5]. Other groups employed frequency domain models using a frequency independent distributed current source per unit length inside the electrical transmission line [12]. Our model uses a quasi-static equivalent circuit for the electrical transmission line with a distributed current source which is more accurately described as the dynamics of the photogenerated carriers are considered. At first, a theoretical analysis based upon the carrier continuity equations is used to describe the frequency dependent distributed photo current generated at any point along the detector. This current includes the intrinsic effects such as the transit time limitation due to the propagation through the intrinsic layers. Next, a model based upon the transmission line method (TLM) is used in order to describe the contribution of the distributed photo current to the total electrical power delivered to the load impedance. Limiting effects due to the electrical wave propagation along the hybrid coplanar/microstrip transmission line of the TW-PD are included in the TLM model. To verify the reliability of the developed model, the theoretical calculations are compared with the experimental results and the limiting contributions of the different physical effects are identified.

Fundamentally, the photogenerated carrier transport in the TW-PD waveguide structure is described by the continuity equation. By neglecting the transversal carrier transport and assuming harmonic time dependence, the one-dimensional (1-D) complex continuity equations for the electron and hole densities $n(x)$ and $p(x)$ are given by

$$j\omega \cdot n(x) = D_n \cdot \frac{\delta^2}{\delta x^2} n(x) - \frac{\delta}{\delta x}\left[n(x) \cdot v_n(x)\right] - R_c + G_c \tag{2}$$

$$j\omega \cdot p(x) = D_p \cdot \frac{\delta^2}{\delta x^2} p(x) - \frac{\delta}{\delta x}\left[p(x) \cdot v_p(x)\right] - R_c + G_c. \tag{3}$$

The first term in the continuity equations describes the carrier diffusion with the electron and hole diffusion constants represented by D_n and D_p. These diffusion constants are functions of carrier velocity and electric field and it has been shown [10], that the carrier diffusion constants get very small in value for high electric fields in excess of 20 kV/cm. Assuming that the typical thickness of a high-frequency p-i-n detector is well below 1 μm and assuming further that a reverse voltage of a few volts is applied, strong electric fields well above 20 kV/cm occur. Thus, for calculating the photogenerated current we can neglect carrier diffusion in the intrinsic region of the reverse biased TW-PD. The second term in (2) and (3) describes the carrier drift in the presence of an electric field with $v_n(x)$ and $v_p(x)$ representing the electron and hole velocity, respectively. The carrier recombination rate represented by R_c can also be neglected for our purposes, since the carrier lifetime in InGaAsP strained MQWs is in the order of a few nanoseconds [13] which is about three orders of magnitude larger than the average transit time of the investigated structure. The last term G_c, representing the carrier generation rate, is a function of the optical intensity at any point along the detector and it can be determined to be

$$G_c = G_0 \cdot \exp(-\gamma_{\text{opt}} \cdot z) \tag{4}$$

with

$$G_0 = \frac{\eta \cdot \lambda}{h \cdot c} \cdot \alpha_{\text{opt}} \cdot I_{\text{opt}}. \tag{5}$$

Here η denotes the external quantum efficiency, γ_{opt} is the complex propagation constant of the optical heterodyne input signal and I_{opt} represents the optical intensity. It should be noted that the carrier generation rate is a function of the longitudinal coordinate z due to the optical wave propagation determined by the complex heterodyne optical propagation constant γ_{opt}.

The electron and hole current densities can be calculated from

$$J_n(x) = -q \cdot v_n(x) \cdot n(x) \tag{6}$$

$$J_p(x) = -q \cdot v_p(x) \cdot p(x). \tag{7}$$

Here we assume that electrons and holes in the intrinsic region travel at constant saturation velocity v_n and v_p, an assumption neglecting carrier escape times which is valid and appropriate

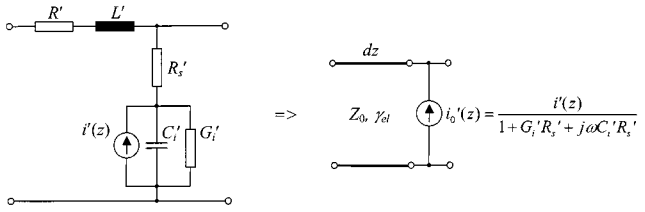

Fig. 7. Quasi-static equivalent transmission line circuit for unit length TW-PD.

for reverse biased TW-PDs with strong internal electric fields. Although there exists some uncertainty about the absolute carrier escape times in reverse-biased MQW structures, experimental investigations have been published demonstrating that the carrier escape times drastically decrease with the bias field indicating that carrier escape times for strong reverse-biased structures are below 1 ps [16], [17].

By solving the differential equations (2) and (3) for the investigated TW-PD structure (see Fig. 2) the electron and hole carrier densities are found. Substituting this result into (6) and (7), we gain the total photo current per unit length generated at any point z along the TW-PD

$$i'(z) = \frac{w}{d_{in}+d_{ip}+d_0}\cdot\frac{q\cdot G_0\cdot\exp(-\gamma_{\rm opt}\cdot z)}{j\omega} \cdot \left[\begin{array}{l} v_n\cdot\left(\frac{v_n}{j\omega}-d_0-\frac{v_n}{j\omega}\cdot\exp\left(-j\omega\cdot\frac{d_0}{v_n}\right)\right) \\ +v_p\cdot\left(\frac{v_p}{j\omega}-d_0-\frac{v_p}{j\omega}\cdot\exp\left(-j\omega\cdot\frac{d_0}{v_p}\right)\right) \\ +v_n\cdot\left(\exp\left(-j\omega\cdot\frac{d_0}{v_n}\right)-1\right) \\ \cdot\left(\frac{v_n}{j\omega}-\frac{v_n}{j\omega}\cdot\exp\left(-j\omega\cdot\frac{d_{in}}{v_n}\right)\right) \\ +v_p\cdot\left(\exp\left(-j\omega\cdot\frac{d_0}{v_p}\right)-1\right) \\ \cdot\left(\frac{v_p}{j\omega}-\frac{v_p}{j\omega}\cdot\exp\left(-j\omega\cdot\frac{d_{ip}}{v_p}\right)\right) \end{array}\right]. \quad (8)$$

This equation not only comprises the carrier transport and generation within the intrinsic absorptive layer of the TW-PD but also the carrier transport through the adjacent nonabsorptive intrinsic regions of the waveguide core (see Fig. 2).

In the next step, we need to develop a model describing the contribution of the distributed current source to the overall electrical wave propagating along the transmission line of the TW-PD. The type of transmission line formed in this TW-PD is a slow-wave hybrid coplanar/microstrip waveguide [14]. Generally, such transmission lines require "full-wave" analysis for rigorous modeling [15]. However, for our purposes the quasi-TEM analysis using a quasi-static equivalent circuit model as shown in Fig. 7(a) satisfactorily describes the millimeter-wave properties of the TW-PD transmission line. Here, the photogenerated current per unit length is represented by the current source $i'(z)$. R' and L' are the resistance and the inductance of the metal center conductor per unit length, respectively. R'_s represents the semiconductor losses associated with transverse current flow in the doped cladding layers and C'_i and G'_i are the capacitance and the conductance of the intrinsic core layer per unit length. The air capacitance which is typically very small in value is neglected. By transforming the current source $i'(z)$, we can convert the equivalent circuit into a form where the active current source is in parallel to the completely passive electrical transmission line of unit length represented by its characteristic impedance Z_0 and propagation constant γ_{el} [Fig. 7(b)]. For the transformed current source $i'_0(z)$ and the relevant microwave properties of the TW-PD we obtain

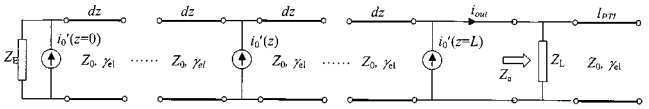

Fig. 8. TLM model describing the distributed current generation along the TW-PD.

$$i'_0(z) = \frac{i'(z)}{1+R'_s\cdot G'_i+j\omega\cdot C'_i\cdot R'_s} = i'_0\cdot\exp(-\gamma_{\rm opt}\cdot z), \quad (9)$$

$$Z_0 = \sqrt{\frac{R'+j\omega\cdot L'}{\left(\frac{G'_i+j\omega\cdot C'_i}{1+R'_s\cdot G'_i+j\omega\cdot C'_i\cdot R'_s}\right)}} \quad (10)$$

$$\gamma_{el} = \sqrt{(R'+j\omega\cdot L')\cdot\left(\frac{G'_i+j\omega\cdot C'_i}{1+R'_s\cdot G'_i+j\omega\cdot C'_i\cdot R'_s}\right)}. \quad (11)$$

The contribution of the distributed photogenerated current $i'_0(z)$ at any point of the detector to the overall current propagating along the transmission line can be described by the transmission line model (TLM) as shown in Fig. 8. Here Z_E represents the impedance at the input port and Z_L is the load impedance of the coplanar probes at the output port. In order to increase the output power of a traveling-wave PD delivered to the load impedance, it is a fundamental requirement to reduce the millimeter-wave reflections at the output port. However, in millimeter-wave measurements using commercially available coplanar probes the load impedance Z_L is fixed to 50 Ω, an impedance that is significantly larger than the typical characteristic impedance Z_0 of ultrahigh frequency TW-PDs which is typically in the range of 10–20 Ω. To overcome this impedance mismatch in the experiment an open ended long ($l_{\rm PTL} = 450$ μm) passive transmission line with a characteristic impedance Z_0 is used in parallel to the load impedance Z_L. This way the impedance mismatch at the output port is reduced keeping in mind, that the power delivered to Z_L is of course not the total power generated by the TW-PD.

Based on the TLM model, the RF output power delivered to the load impedance Z_L can be analytically determined by (12), shown at the bottom of the following page, with

$$r_e = \frac{Z_E - Z_0}{Z_E + Z_0} \quad (13)$$

and

$$r_a = \frac{Z_a - Z_0}{Z_a + Z_0} \quad (14)$$

representing the reflection coefficients at the input and output ports, respectively.

The presented frequency domain model allows to consider the relevant limiting intrinsic effects such as transit times limitations as well as limitations due to propagation effects such as microwave losses and the mismatch between the optical group velocity and the electrical phase velocity. By applying this model to the investigated TW-PD, the contribution of the different effects on the total rolloff at high-frequencies can be identified and the impact of design variations of the high-frequency performance can be studied in detail.

In order to numerically calculate the generated power the circuit parameters of the TW-PD equivalent circuit must be determined first. Generally, these parameters are frequency dependent but for frequencies in excess of 20 GHz the parameters L', R'_s, C'_i and G'_i are considered to be constant. Only R' increases with the square root of frequency due to the skin effect. In good approximation C'_i can be determined by $C'_i = \varepsilon_0\varepsilon_\rho \cdot w/d_i$ resulting in 1.7 pF/mm for the investigated TW-PD structure. The constant conductor resistance per unit length at frequencies below 10 GHz is given by $R' = \rho_{Au}/(w \cdot d_{met})$ resulting in 18.5 Ω/mm. For frequencies in excess of 10 GHz R' is considered to increase with the square root of the frequency. The series resistance of the doped semiconductor layers for a 6 -μm-wide rib waveguide with 15 -μm separation between the center and the ground electrode is approximately $R'_s \sim 0.25$ Ω·mm. The parallel conductance $G'_i \sim 20$ mS/mm and the transversal inductance $L' \sim 0.1$ nH/mm were experimentally determined from S-parameter measurements. With all the equivalent circuit parameters known, the complex characteristic impedance Z_0 and the complex electrical propagation constant γ_{el} of the TW-PD transmission line can be calculated. The theoretically determined complex characteristic impedance for microwave frequencies is shown in Fig. 9 and it is compared with experimental values obtained from on-wafer S-parameter measurements. As can be seen, there is a good agreement between the experimental and theoretical data indicating that the approximations used to determine the equivalent circuit parameters are appropriate.

In Fig. 10, the theoretically determined characteristic impedance and the propagation constant are plotted up to 200 GHz millimeter-wave frequency.

In Fig. 11 the theoretically calculated power delivered to the load impedance Z_L is compared with the experimental data already presented in Fig. 3. The excellent agreement between measured and simulated data with a maximum variation of only 3 dB proves the accuracy and reliability of the analytical model. The total rolloff for a frequency span from 20 to 200 GHz is 13.1 dB. For future design optimizations with respect to a higher

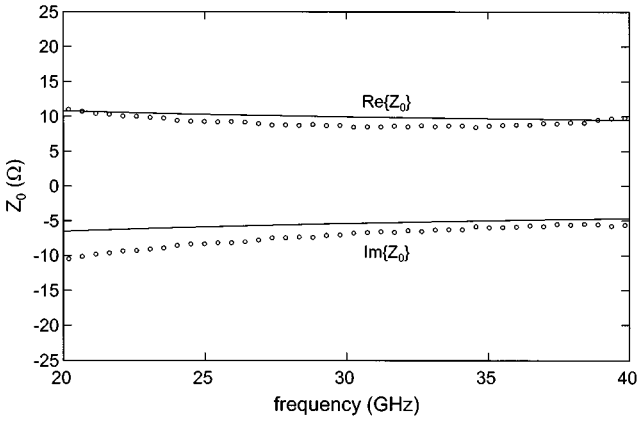

Fig. 9. Experimentally (circles) and numerically (solid lines) determined characteristic impedance of the hybrid coplanar/microstrip transmission line.

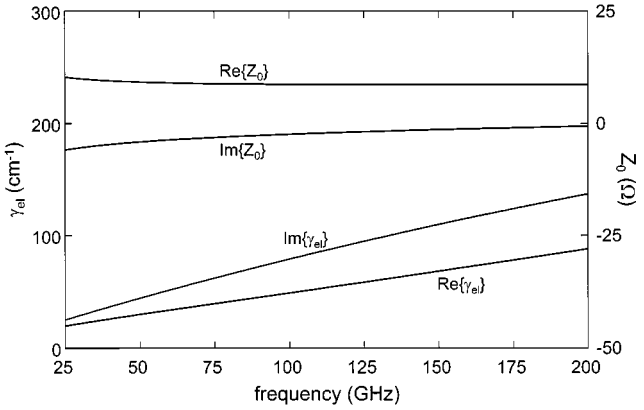

Fig. 10. Theoretically determined characteristic impedance and electrical propagation constant of the hybrid coplanar/microstrip transmission line.

electrical output power, it is of great importance to identify the physical reasons causing this rolloff. By identifying the contributions of the different physical phenomena considered in the developed model, we can state that the total rolloff is composed of a 6.5-dB penalty due to transit time effects and a 1.1-dB penalty due to intrinsic effects resulting from carrier transport in the doped sections of the TW-PD. The remaining penalty of 5.5 dB originates from propagation effects namely microwave losses and velocity mismatch. In order to further improve the TW-PD performance one has to address primarily the penalty caused by transit time and wave propagation effects. A more detailed discussion on the optimization of the p-i-n TW-PD design for high-power (sub)millimeter-wave generation will be presented elsewhere.

$$P_{\text{out},el} = \frac{i_0^2 \cdot Z_L}{8} \cdot \left[\begin{array}{l} \dfrac{1}{\gamma_{el} - \gamma_{\text{opt}}} \cdot \left(\exp(-\gamma_{\text{opt}} \cdot l) - \exp(-\gamma_{el} \cdot l) \right) \\ -\dfrac{r_a}{\left(1 - r_a \cdot r_e \cdot \exp(-2 \cdot \gamma_{el} \cdot l)\right) \cdot (3 \cdot \gamma_{el} - \gamma_{\text{opt}})} \cdot \left(\exp(-\gamma_{\text{opt}} \cdot l) - \exp(-3 \cdot \gamma_{el} \cdot l) \right) \\ -\dfrac{r_e}{\left(1 - r_a \cdot r_e \cdot \exp(-2 \cdot \gamma_{el} \cdot l)\right) \cdot (\gamma_{el} + \gamma_{\text{opt}})} \cdot \left(\exp(-\gamma_{\text{opt}} \cdot l - 2 \cdot \gamma_{el} \cdot l) - \exp(-\gamma_{el} \cdot l) \right) \end{array} \right]^2 \quad (12)$$

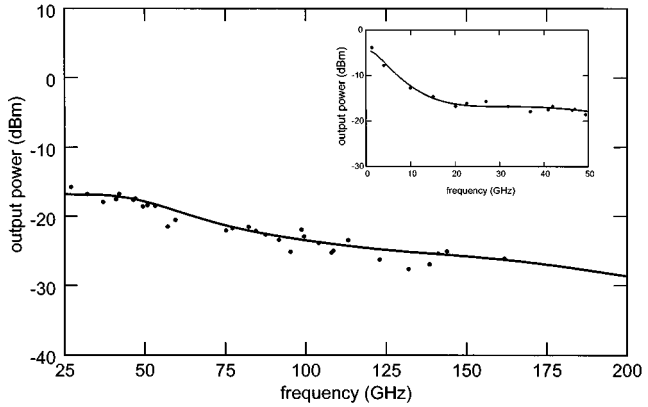

Fig. 11. Experimentally (circles) and numerically (solid line) determined broad-band millimeter-wave generation using the TW-PD. Inset shows comparison between simulated and experimentally determined output power at low frequencies up to 50 GHz.

As discussed earlier, the measured and calculated power shown in Fig. 11 represents the power delivered to the probe. It does not represent the total power generated by the TW-PD. Referring to Fig. 10, the absolute value of the characteristic impedance at 110 GHz is $Z_0 = 9\ \Omega$. Thus, the total power generated by the TW-PD is estimated to be 8.16 dB larger than the measured power delivered to the probes.

V. Conclusion

In summary, we have presented to the best knowledge of the authors the first experimental demonstration of optical heterodyne millimeter-wave generation up to 160 GHz using a ultrahigh frequency TW-PD with a record measured millimeter-wave power of -11.5 dBm at 110 GHz. The total power generated by the detector is estimated to be about 8 dB larger. Both, the generated maximum output power and the maximum frequency are currently limited by the experimental setup. Furthermore, we presented a theoretical analysis for describing the high-frequency limitations of TW-PD such as transit times, microwave losses, and velocity mismatch. An excellent agreement between the experimentally and theoretically determined values is found indicating a total rolloff of 13.1 dB for a frequency span from 20 to 200 GHz. This rolloff is found to be mainly due to transit time limitations and microwave losses.

Acknowledgment

The authors would like to thank M. Schneider and R. Buß of Gerhard-Mercator Universität Duisburg, ZHO-Optoelektronik, for their valuable support. The authors also like to thank J. Payne of the National Radio Astronomy Observatory, Tucson, AZ, and R. Güsten of the Max Plank Institut für Radioastronomie, Bonn, Germany, for their encouragement.

References

[1] J. Soohoo, S.-K. Yao, J. E. Miller, R. R. Shurtz, II, Y. Taur, and R. A. Gudmundsen, "A laser-induced traveling-wave device for generating millimeter-waves," *IEEE Trans. Microwave Theory Tech.*, vol. MTT-29, pp. 1174–1182, Nov. 1981.

[2] J. Payne, B. Shillue, and A. Vaccari, "Photonic techniques for the atacama large millimeter array," in *Proc. Int. Microwave Photon. Topical Meeting*, Melbourne, Australia, Nov. 1999, pp. 105–108.

[3] D. Wake, C. R. Lima, and P. A. Davis, "Optical generation of millimeter-wave signals for fiber-rado systems using a dual-mode DFB semiconductor laser," *IEEE Trans. Microwave Theory Tech.*, vol. 43, pp. 2270–2276, Sept. 1995.

[4] A. Stöhr, R. Heinzelmann, K. Kitayama, T. Kuri, and D. Jäger, "Photonics for millimeter-wave broadband wireless," in *Proc. SPIE Terahertz Gigahertz Electron. Photon. II*, vol. 4111, J. Hwu and K. Wu, Eds., Aug. 2000, pp. 1–6.

[5] K. Kato, "Ultrawide-band/high-frequency photodetectors," *IEEE Trans. Microwave Theory Tech.*, vol. 47, pp. 1265–1281, July 1999.

[6] T. Nagatsuma, A. Hirata, Y. Royter, M. Shinagawa, T. Furuta, T. Ishibashi, and H. Ito, "A 120GHz Integrated photonic transmitter," in *Proc. Int. Microwave Photon. Topical Meeting*, U.K., Sept. 2000, pp. 225–228.

[7] M. Alles, U. Auer, F.-J. Teude, and D. Jäger, "Distributed velocity matched 1.55-μm InP traveling-wave photodetector for generation of high millimeterwave signal power," in *IEEE MTT-S Int. Microwave Symp. Dig.*, Baltimore, MD, 1998, pp. 1233–1236.

[8] T. Chau, N. Kaneda, T. Jung, A. Rollinger, S. Mathai, Y. Qian, T. Itoh, M. C. Wu, W. B. Shillue, and J. M. Payne, "Generation of millimeter waves by photomixing at 1.55 μm using InGaAs–InAlAs–InP velocity-matched distributed photodetectors," *IEEE Photon. Technol. Lett.*, vol. 12, pp. 1055–1057, Aug. 2000.

[9] A. Stöhr, R. Heinzelmann, C. Kaczmarek, and D. Jäger, "Ultra-broadband K_a- to W-band 1.55 μm travelling-wave photomixer," *Electron. Lett.*, vol. 36, no. 11, pp. 970–972, May 2000.

[10] Y.-L. Huang and C. K. Sun, "Nonlinear saturation behaviors of high-speed p-i-n photodetectors," *J. Lightwave Technol.*, vol. 18, pp. 203–212, Feb. 2000.

[11] K. S. Giboney, J. W. Rodwell, and J. E. Bowers, "Traveling-wave photodetector theory," *IEEE Trans. Microwave Theory Tech.*, vol. 45, pp. 1310–1319, Aug. 1997.

[12] V. Hietala, G. A. Vawter, T. M. Brennan, and B. E. Hammons, "Traveling-wave photodetectors for high-power, large-bandwidth applications," *IEEE Trans. Microwave Theory Tech.*, vol. 43, pp. 2291–2298, Sept. 1995.

[13] D. X. Zhu, S. Dubovitsky, W. H. Steier, J. Burger, D. Tishinin, K. Uppal, and D. Dapkus, "Ambipolar diffusion coefficient and carrier lifetime in a compressively strained InGaAsP multiple quantum well device," *Appl. Phys. Lett.*, vol. 71, no. 5, pp. 647–649, Aug. 1997.

[14] D. Jäger, "Slow-wave propagation along variable Schottky-contact microstrip line," *IEEE Trans. Microwave Theory Tech.*, vol. MTT-24, pp. 566–573, Sept. 1976.

[15] P. Berini, A. Stöhr, K. Wu, and D. Jäger, "Normal mode analysis and characterization of an InGaAs/GaAs MQW field-induced optical waveguide including electrode effects," *J. . Lightwave Technol.*, vol. 14, pp. 2422–2435, Oct. 1996.

[16] K. J. Williams, R. D. Esman, and M. Dagenais, "Effects of high space-charge fields on the response of microwave photodetectors," *IEEE Photon. Technol. Lett.*, vol. 6, pp. 639–641, June 1994.

[17] H. Hillmer and S. Marcinkevièius, "Optically detected careir transport in III/V semiconductor QW structures: Experiments, model calculations and applications in fast 1.55 μm laser devices," *Appl. Phys. Lett. B*, vol. 66, pp. 1–17, 1998.

Andreas Stöhr (M'97) received the Dipl.-Ing. and Dr.-Ing. degrees in electrical engineering from Gerhard-Mercator-University Duisburg (GMUD), Duisburg, Germany, in 1991 and 1997, respectively.

Since 1995, he has been a Staff Member of the Optoelectronics Department, GMUD. In 1998, he joined the Communications Research Laboratory (CRL), Ministry of Posts and Telecommunications, Tokyo, Japan. His current research interests include the design and fabrication of III/V-based microwave photonic devices and their application in microwave or millimeter-wave fiber-optic transmission systems, as well as in optical sensors. He has published more than 70 papers in refereed journals and conferences.

Dr. Stöhr is a member of the IEEE Laser and Electro-Optics Society (LEOS) and the IEEE Microwave Theory and Techniques Society (IEEE MTT-S). He is a member of the National Organizing Committee for Photonics in Measurements. He was a member of the organizing committee for the International Topical Meeting on Microwave Photonics MWP'97. He received the 1997 Annual Award from the Duisburger Universitäts Gesellschaft.

Robert Heinzelmann received the Dipl.-Ing. degree in electrical engineering from the Gerhard-Mercator-Universität Duisburg (GMUD), Duisburg, Germany, in 1992, and is currently working toward the Ph.D. degree at the GMUD. His Dipl.-Ing. thesis dealt with the development of planar phased-array antennas for millimeter-wave applications.

In 1993, he continued his research on microwave and millimeter-wave circuits and devices as a Junior Research Assistant with the Department of Electrical and Computer Engineering, University of Victoria, Victoria, BC, Canada. In 1994, he joined the Department of Optoelectronics, GMUD. He is also in charge of the 250-m^2 cleanroom facilities of the Department of Optoelectronics. In 1999, he was with the Communications Research Laboratory, Ministry of Posts and Telecommunications, Tokyo, Japan, as Visiting Scientist. He has authored or co-authored more than 40 refereed journal and conference papers. His research interests include optical communication and sensing systems, with the main focus on the development of high-speed III–V semiconductor components, especially waveguide modulators and photomixers.

Andrei Malcoci received the Dipl.-Ing degree in electrical engineering from the Politehnica-University-Timisooara (UTT), Timisooara, Romania, in 1997, and the DEA degree in automation and industrial computer science from the Université de Haute-Alsace (UHA), Mulhouse, France, in 1998.

In 1997, he joined the TROP Group, Mulhouse, France, where he conducted research in the field of neural networks. From 1998 to 2000, he was an IT Engineer involved with various projects in industry. In 2000, he joined the Optoelectronics Department, Gerhard-Mercator-University Duisburg (GMUD), Duisburg, Germany. He has authored three papers in refereed journals and conferences. His current research interests include the design and fabrication technology of III–V-based millimeter-wave photonic devices.

Dieter Jäger (F'01) received the Diplomphysiker, Dr.rer.nat., and Habilitation degrees in physics from the Westfalische Wilhelms-Universität Munster, Munster, Germany, in 1969, 1974, and 1980, respectively.

From 1974 to 1990, he was Head of a research group at the Institute for Applied Physics, where he became an Associate Professor of physics in 1985. From 1989 to 1990, he was a Visiting Professor at the University of Duisburg, Duisburg, Germany. Since 1990, he has been with the Faculty of Electrical Engineering, University of Duisburg, where he is Head of the Department of Optoelectronics. Since 1998, he has also been the Dean of the Faculty. He is currently engaged in nonlinear phenomena in solid-state devices for MMIC applications, as well as nonlinear optics, ultrafast electrooptics, and optical switching in semiconductors for optoelectronic signal processing. He is a Honorary Professor of the Brasov University/Romania and a Consultant Professor of the Huozhong University of Science and Technology, Huozhong, China. He has authored or co-authored over 200 papers in books, journals, and conferences proceedings and is a reviewer for several journals. His research interests include ultrafast optoelectronics for microwave power generation and transmission, millimeter-wave optical links for broad-band communication technologies, and picosecond electrooptical measuring techniques. He is also active in the areas of optical neural technology and optoelectronics for medical applications. He is a correspondent of the Union Radio-Scientifique Internationale (URSI).

Prof. Jäger is a chair of the German IEEE Lasers and Electro-Optics Society (IEEE LEOS) chapter. He is a member of the IEEE Microwave Photonics Steering Committee and is also a member of the German Physical Society (DPG), the German Vacuum Association (DVG), the German Society of Information Technology (VDE, ITG), and the German Association for Applied Optics (DGaO).